ON THE SCALING OF THE ENERGY GAIN OF ICF TARGETS

M.M. BASKO*
Joint Institute for Laboratory Astrophysics,
National Institute of Standards and Technology,
and University of Colorado, Boulder, Colorado,
United States of America
and
Institute for Theoretical and Experimental Physics,
Moscow, Russian Federation**

ABSTRACT. A new gain model based on an adiabatic self-similar solution of the hydrodynamic equations is proposed for inertial confinement fusion (ICF) targets ignited by means of a thermonuclear spark at the fuel centre. The model is applied to analyse gain curves corresponding to fixed values of the implosion velocity U_{im}. It is shown that the adequate ignition criterion, allowing for the inertia of the cold fuel, implies $\rho_s R_s T_s \propto U_{im}$ at the time of ignition, as contrasted to fixed values of the spark areal density, $\rho_s R_s$, and the temperature, T_s, assumed in many of the earlier publications. The modified ignition condition leads to the scaling $E_{min} \propto \alpha^3 U_{im}^{-7}$ and $G_f^* \propto (E/\alpha^3)^{0.4}$ for the ignition energy threshold, E_{min}, and the limiting fuel gain, G_f^*, of ICF capsules; α is the isentrope parameter of the cold fuel, E is the energy invested in the DT fuel. Stability and symmetry constraints do not affect this scaling when the initial aspect ratio of the fusion capsule $A_0 \gg 1$; in the opposite case of initially thick capsule shells, the scaling of E_{min} and G_f^* with U_{im} and α becomes ill defined.

1. INTRODUCTION

As in many branches of physics, scaling laws play an important role in inertial confinement fusion (ICF) research. On the one hand, they represent the basic physics governing a phenomenon under consideration. On the other hand, scaling relationships help to save much effort and computing time when, for example, an ICF target designed for a specific set of external parameters can simply be rescaled to other values of these parameters. In ICF research, special attention has always been paid to the scaling of the target energy gain G with the input driver energy E_{dr}.

In recent publications by the Livermore group [1–4], the dependence of G on E_{dr} has been discussed as a family of separate gain curves corresponding to different values of the implosion velocity U_{im}. The underlying physics is based on the following similarity law, which with good accuracy holds for indirectly driven fusion capsules. If, for given initial densities, all the dimensions of a fusion capsule are scaled down (up) by the same factor X, while the temperature of the driving X rays (more accurately, the pressure and the rate of ablation) is kept constant and only the pulse profile is compressed (stretched) by the same factor X, the capsule implodes along the same sequence of states in the ρ, T plane and reaches the same implosion velocity U_{im} and the same maximum density and temperature at the time of stagnation. Evidently, the constituent masses and the input energy scale as X^3. Also, implosions scaled in this way preserve the values of the convergence ratio, as well as the initial and the inflight aspect ratios of the capsule layers — which means that they all have roughly the same stability limitations and symmetry requirements. Thus, a gain curve $G(E_{dr})$ obtained for a fixed value of the implosion velocity should adequately represent a family of capsules with different sizes driven by radiation field with a fixed X ray temperature. Any such curve has an ignition threshold $E_{dr,min}$ because, for a fixed U_{im}, it is impossible to satisfy the condition of inertial confinement for arbitrarily small fuel masses. An important issue is the scaling of $E_{dr,min}$ with the implosion velocity and other relevant parameters. The envelope of the gain curves for different U_{im} is the limiting gain curve $G^* = G^*(E_{dr})$.

Earlier, a number of attempts have been made to derive scaling laws for G^* and $E_{dr,min}$ by simply analysing the deuterium–tritium (DT) fuel states at the time of maximum compression. The published gain models are based on either a constant density [5, 6], a constant pressure [7, 8] or more realistic analytic [9] profiles across the

* JILA Visiting Fellow in 1992–1993.
** Permanent affiliation.

spark and cold fuel regions. All such models assume a fixed coupling efficiency η_f between the driver energy E_{dr} and the energy $E = \eta_f E_{dr}$ invested in the fuel and, using the relationship $G(E_{dr}) = \eta_f G_f(\eta_f E_{dr})$, identify the scaling of the target gain $G(E_{dr})$ with the scaling of the fuel gain $G_f(E)$. However, the results obtained in this manner significantly differ from those that were published by the Livemore group [1–4] and are based on sophisticated numerical simulations. A better agreement — though in a limited range of parameters — was achieved in Refs [10, 11] after constraints due to the hydrodynamic instabilities and to the drive asymmetries had been introduced by assuming fixed values of the radial convergence ratio and the initial aspect ratio for the fuel shell. On the other hand, it is well known [12, 13] that the stability constraints limit the inflight rather than the initial aspect ratio of imploding shells. Thus, the problem appears to deserve a more thorough examination.

Here, we propose a new parametrization scheme for the DT fuel states near ignition based on the self-similar solution for adiabatic contraction and expansion of a gaseous sphere. Besides being more accurate than the isochoric and isobaric approximations, this parametrization enables us to establish an adequate scaling for spark parameters at ignition with the implosion velocity, $\rho_s R_s T_s \propto U_{im}$, as contrasted to the widely used condition of fixed $\rho_s R_s$ and T_s. This scaling originates from the tamping effect of the cold fuel and is the key new element in the present work. Although the effect of cold fuel on the ignition criterion has been discussed by a number of authors [8, 14, 15], the link between the spark parameters at ignition and the implosion velocity appears to have eluded proper recognition. By using the ignition criterion in this way modified, we infer the scaling $E_{min} \propto \alpha^3 U_{im}^{-7}$, which is confirmed by direct one dimensional simulations of the ignition of DT spheres and agrees better with the Livermore results [2–4] than the relationship $E_{min} \propto \alpha^3 U_{im}^{-10}$ derived in Ref. [16] under the isobaric approximation with fixed spark parameters $\rho_s R_s$ and T_s; here, α is the isentrope parameter of the cold fuel. If symmetry and stability constraints are imposed as certain fixed values of the radial convergence and the inflight aspect ratios, we find that they modify the above scaling only in the case of large initial thickness of the fusion capsule.

2. FUEL PARAMETRIZATION

To obtain a suitable parametrization of possible DT fuel configurations near the time of ignition, we invoke the following self-similar solution:

$$u(t, r) = \dot{R}\xi \tag{1}$$

$$\rho(t, r) = \rho_0(t)\omega(\xi) \tag{2}$$

$$P(t, r) = P_0(t)\left(1 - \frac{1}{\Omega}\int_0^{\xi} \xi'\omega(\xi')\,d\xi'\right) \tag{3}$$

which describes a homologous adiabatic contraction (expansion) of a gaseous sphere with a prescribed entropy distribution over the mass co-ordinate. This solution belongs to the well studied class of motions with linear velocity profiles [17]. In Eqs (1)–(3),

$$\xi = \frac{r}{R} \tag{4}$$

is the self-similar variable, $R = R(t)$ is the outer fuel radius obeying the equation of motion

$$R\ddot{R} = \frac{1}{\Omega}\frac{P_0(t)}{\rho_0(t)} \tag{5}$$

$\rho_0(t)$ and $P_0(t)$ are, respectively, the central density and the pressure, $\omega(\xi)$ is an arbitrary function defining the DT density (or, equivalently, entropy) profile, and

$$\Omega = \int_0^1 \xi\omega\,d\xi \tag{6}$$

is a dimensionless constant. For the adiabatic index equal to $\frac{5}{3}$, when the ratio $P_0/\rho_0^{5/3}$ is constant, Eq. (5) can be integrated to give

$$\dot{R}^2 = U_\infty^2\left[1 - \left(\frac{R_m}{R}\right)^2\right] \tag{7}$$

$$R(t) = (R_m^2 + U_\infty^2 t^2)^{1/2} \tag{8}$$

where R_m is the fuel radius at the time of stagnation $t = 0$,

$$U_\infty = \left(\frac{P_{0m}}{\Omega\rho_{0m}}\right)^{1/2} = 2.78 \times 10^7 \left(\frac{T_{0m}\,[\text{keV}]}{\Omega}\right)^{1/2} [\text{cm/s}] \tag{9}$$

is the implosion velocity of the outer fuel edge in the limit of $t \to -\infty$, and $\rho_{0m} = \rho_0(0)$, $T_{0m} = T_0(0)$, and $P_{0m} = P_0(0)$ are, respectively, the density, temperature, and pressure in the fuel centre at stagnation.

Here, it should be emphasized that we employ the adiabatic solution (1)–(9) to approximate not the entire process of the fuel implosion, but rather its motion during a short period just before ignition within which the effects of non-adiabatic processes do not have time to accumulate and cause serious flow distortions. Clearly, the dynamically self-consistent pressure and density profiles obtained in this way should be closer to reality than the step-like approximations used in Refs [5–8]. In this work,

we consider only bare DT microspheres, with the boundary pressure $P(t, R) = 0$ (see Eqs (3) and (6)). The self-similar solution (1)–(9) can easily be generalized to include a thin massive pusher at $r = R$ [18]. We avoid this complication, primarily because the results obtained even for moderate values of the pusher to fuel mass ratio $\mu_p \gtrsim 1$–3 seem to be of little practical value for spark ignition near stagnation because of rapid spark dissipation [18] and the Rayleigh–Taylor instability at the pusher/fuel interface.

On the assumption that the fuel ignition is initiated by a thermonuclear spark — a hot region in the fuel centre — we specify the density profile $\omega(\xi)$ by (1) choosing $\omega(\xi) = 1$ inside the spark region $0 < \xi < \xi_s$, and (2) adopting a constant value of the entropy parameter:

$$\alpha \equiv \frac{P(t, r)}{P_{\text{deg}}(t, r)} \tag{10}$$

throughout the cold fuel region $\xi_s < \xi < 1$. Here,

$$P_{\text{deg}} = \frac{1}{5}(3\pi^2)^{2/3}\frac{\hbar^2}{m_e}\left(\frac{\rho}{Am_A}\right)^{5/3}$$
$$= 2.18\ (\rho\ [\text{g/cm}^3])^{5/3}\ [\text{Mbar}] \tag{11}$$

is the cold pressure of the degenerate electron gas in a fully ionized equimolar DT mixture of density ρ. Then

$$\omega(\xi) = \begin{cases} 1 & 0 < \xi < \xi_s \\ 5\dfrac{\Omega - \frac{1}{2}\xi_s^2}{(1 - \xi_s^2)^{5/2}}(1 - \xi^2)^{3/2}, & \xi_s < \xi < 1 \end{cases} \tag{12}$$

The density and pressure profiles given by Eqs (2), (3), and (12) are illustrated in Fig. 1. The density jump at the hot/cold fuel interface is

$$\omega_c = 5\frac{\Omega - \frac{1}{2}\xi_s^2}{1 - \xi_s^2} \tag{13}$$

The total mass and energy of the fuel can be calculated as

$$M = 4\pi\rho_{0m}R_m^3\int_0^1 \omega\xi^2\,d\xi$$
$$= 4\pi\rho_{0m}R_m^3\left[\frac{1}{3}\xi_s^3 + \frac{5}{16}\left(\Omega - \frac{1}{2}\xi_s^2\right)\phi_M\right] \tag{14}$$

$$E = \frac{3}{2}4\pi P_{0m}R_m^3\int_0^1\left(1 - \frac{1}{\Omega}\int_0^\xi \omega\xi'\,d\xi'\right)\xi^2\,d\xi$$
$$= 2\pi\rho_{0m}R_m^3U_\infty^2\int_0^1 \omega\xi^4\,d\xi$$
$$= 2\pi\rho_{0m}R_m^3U_\infty^2\left[\frac{1}{5}\xi_s^5 + \frac{15}{128}\left(\Omega - \frac{1}{2}\xi_s^2\right)\phi_E\right] \tag{15}$$

where

$$\phi_M = \frac{\frac{\pi}{2} - \arcsin\xi_s}{(1 - \xi_s^2)^{5/2}} + \frac{\xi_s}{3}\frac{8\xi_s^4 - 14\xi_s^2 + 3}{(1 - \xi_s^2)^2} \tag{16}$$

$$\phi_E = \frac{\frac{\pi}{2} - \arcsin\xi_s}{(1 - \xi_s^2)^{5/2}} + \frac{\xi_s}{3}\frac{16\xi_s^6 - 24\xi_s^4 + 2\xi_s^2 + 3}{(1 - \xi_s^2)^2} \tag{17}$$

are slowly varying functions of ξ_s only.

Evidently, the energetically most economical solution would be to ignite the DT fuel at the time of stagnation, $t = 0$. In our model, however, we have the possibility of introducing an ignition margin by assuming that the required spark parameters T_s and $H_s = \rho_s R_s$ are achieved somewhat earlier, at $t = t_{ig} < 0$. This provides us with an extra free parameter

$$q = \frac{R_{ig}}{R_m} \equiv \frac{R(t_{ig})}{R(0)} \geq 1 \tag{18}$$

Now, the ignition (ρ_s, T_s) and stagnation (ρ_{0m}, T_{0m}) parameters are related as

$$\rho_{0m} \equiv \rho_0(0) = q^3\rho_0(t_{ig}) \equiv q^3\rho_s \tag{19}$$

$$T_{0m} \equiv T_0(0) = q^2T_0(t_{ig}) \equiv q^2T_s \tag{20}$$

$$\rho_{0m}R_m\xi_s = q^2\rho_sR_{ig}\xi_s \equiv q^2\rho_sR_s \equiv q^2H_s \tag{21}$$

The implosion velocity of the outer fuel edge at ignition is given by

$$\dot{R}(t_{ig}) = -U_\infty(1 - q^{-2})^{1/2} \tag{22}$$

Note that, in actual implosions with $q > 1$, the stagnation parameters R_m, ρ_{0m}, T_{0m} may never be reached because

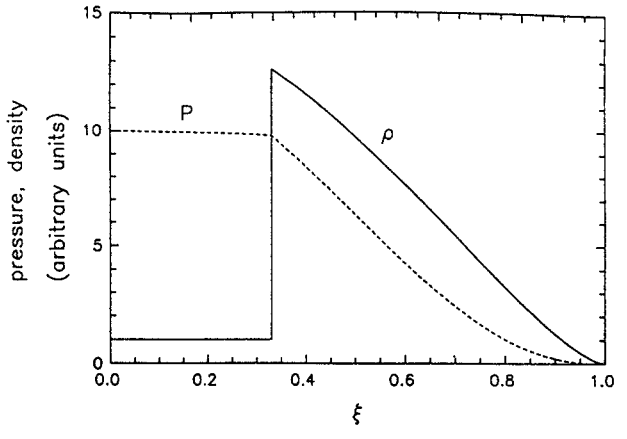

FIG. 1. Radial density (solid curve) and pressure (dashed curve) profiles in the DT fuel according to the self-similar solution (1)–(9), (12).

the fuel explodes on a time-scale much shorter than $|t_{ig}|$. In such cases, the quantities R_m, ρ_{0m}, T_{0m}, P_{0m} should merely be regarded as convenient interim parameters simplifying the calculations.

Thus, according to our model, the fuel state near the time of ignition is fully specified by the values of the following six parameters:

$$U_{im}\ [10^7\ \text{cm/s}],\ H_s\ [\text{g/cm}^2],\ T_s\ [\text{keV}],\ \alpha,\ \xi_s,\ q \qquad (23)$$

The velocity U_∞ given by Eq. (9) differs from what is usually meant as the implosion velocity U_{im}. We relate U_{im} to U_∞ by assuming that the kinetic energy of the cold fuel in the limit $t \to -\infty$ is $\frac{1}{2}M_c U_{im}^2$, where M_c is the mass of the cold fuel given by the second term in brackets on the right hand side of Eq. (14). Then, from Eqs (14) and (15), we obtain

$$U_\infty = U_{im}\left(\frac{8}{3}\frac{\phi_M}{\phi_E}\right)^{1/2} \qquad (24)$$

Explicit expressions for the key quantities in the solution (1)–(9) in terms of the six basic parameters (23) can be obtained as follows:

First, we notice that Eqs (9), (20), and (24) yield

$$\Omega = 2.9\,q^2\,\frac{T_s}{U_{im}^2}\,\frac{\phi_E}{\phi_M} \qquad (25)$$

Here and below, in all practical formulas the values of T_s, H_s, and U_{im} are in units given by Eq. (23). Equating the pressure

$$P(\xi_s - 0)\ [\text{Mbar}] = 772\,\rho_s T_s\left(1 - \frac{\xi_s^2}{2\Omega}\right) \qquad (26)$$

of the hot fuel to the pressure

$$P(\xi_s + 0)\ [\text{Mbar}] = 2.18\,\alpha\rho_s^{5/3}\omega_c^{5/3} \qquad (27)$$

of the cold fuel at the hot/cold interface $\xi = \xi_s$ (ρ_s is in g/cm^3), we calculate the value of the spark density:

$$\rho_s\ [\text{g/cm}^3] = 8.36\,\frac{U_{im}^5}{\alpha^{3/2}q^5 T_s}\,\frac{(1-\xi_s^2)^{5/2}}{1-(2\Omega)^{-1}\xi_s^2}\left(\frac{\phi_M}{\phi_E}\right)^{5/2} \qquad (28)$$

The outer fuel radius at ignition is given by

$$R_{ig} = \frac{H_s}{\rho_s \xi_s} \qquad (29)$$

Using Eqs (18), (19), (21) and (24) to calculate R_m, ρ_{0m} and U_∞, we obtain the following expressions for the mass M and the energy E of the DT fuel:

$$M\ [\text{mg}] = 163\,\frac{\alpha^3 q^{12}(H_s T_s)^3}{U_{im}^{12}}\,\Lambda_M \qquad (30)$$

$$E\ [\text{MJ}] = 0.813\,\frac{\alpha^3 q^{12}(H_s T_s)^3}{U_{im}^{10}}\,\Lambda_E \qquad (31)$$

where

$$\Lambda_M = \frac{[1-(2\Omega)^{-1}\xi_s^2]^3}{\xi_s^3(1-\xi_s^2)^5}\left(\frac{\phi_E}{\phi_M}\right)^6\left(\phi_M + \frac{16}{15}\,\frac{\xi_s^3}{\Omega - \frac{1}{2}\xi_s^2}\right) \qquad (32)$$

$$\Lambda_E = \frac{[1-(2\Omega)^{-1}\xi_s^2]^3}{\xi_s^3(1-\xi_s^2)^5}\left(\frac{\phi_E}{\phi_M}\right)^5\left(\phi_E + \frac{128}{75}\,\frac{\xi_s^5}{\Omega - \frac{1}{2}\xi_s^2}\right) \qquad (33)$$

The areal density of the cold fuel at ignition can be expressed as

$$H_c\ [\text{g/cm}^2] = 5.43\,q^2\,\frac{H_s T_s}{U_{im}^2}\,\Lambda_H \qquad (34)$$

where

$$\Lambda_H = \left(1 - \frac{\xi_s^2}{2\Omega}\right)\left[\frac{\frac{\pi}{2} - \arcsin\xi_s}{\xi_s(1-\xi_s^2)^{5/2}} + \frac{1}{3}\,\frac{2\xi_s^2 - 5}{(1-\xi_s^2)^2}\right]\frac{\phi_E}{\phi_M} \qquad (35)$$

The dependence of Λ_M, Λ_E, and Λ_H on ξ_s is illustrated in Fig. 2. Equations (30)–(35) serve as the basis for the scaling relationships to be derived below.

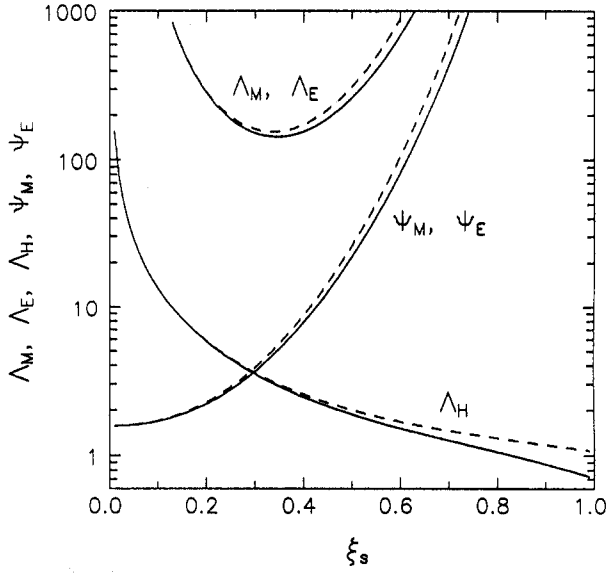

FIG. 2. Dimensionless functions Λ_M, Λ_E, Λ_H, Ψ_M, and Ψ_E as defined by Eqs (32), (33), (35), (54), and (55) plotted versus fractional spark radius ξ_s for two values of the parameter Ω: solid curves — $\Omega = 1$, dashed curves — $\Omega = 2$. In both cases, Λ_M coincides with Λ_E, and Ψ_M coincides with Ψ_E within the thickness of corresponding curves.

3. SCALING RELATIONSHIPS

3.1. Ignition at a fixed threshold for spark parameters

The simplest criterion for ignition that was used in most of the earlier publications on the gain scaling [2, 5-7, 9-11] is to assume that the DT fuel ignites upon reaching certain fixed values of the spark temperature, T_s, and areal density, $H_s = \rho_s R_s$. Here, we slightly modify this criterion to

$$\begin{cases} T_s > 5 \text{ keV} \\ H_s T_s = 2 \text{ g}\cdot\text{cm}^{-2}\cdot\text{keV} \end{cases} \tag{36}$$

On the one hand, a fixed value of the product $H_s T_s$ corresponds to a physically more adequate threshold for spark ignition than separately fixed values of H_s and T_s [15, 19] because it accounts for hot narrow sparks which initially dissipate (evolving with approximate conservation of the $H_s T_s$ products; see Appendix A) because of the electron heat conduction and ignite only later. On the other hand, the key expressions (30), (31), and (34) contain H_s and T_s in the combination $H_s T_s$ only.

If we restrict our analysis to implosion velocities $U_{im} \leq 5 \times 10^7$ cm/s and fractional spark radii $\xi_s \leq 0.5$, then the weak dependence of Λ_M, Λ_E, and Λ_H on Ω can be ignored, and the fuel mass M, energy E, and the cold fuel areal density H_c in Eqs (30), (31), and (35) become fully factorized functions of the six basic parameters (23). Moreover, the two functions $\Lambda_M(\xi_s)$ and $\Lambda_E(\xi_s)$ are practically equal in this parameter region (Fig. 2) and both achieve minima $\Lambda_{M,\min} \approx \Lambda_{E,\min} = \Lambda_m \approx 150$ at $\xi_s \approx 0.34$. Combining this result with the ignition criterion (36) and assuming $q = 1$ (ignition at stagnation), from Eq. (30) we obtain the following expression for the minimum DT mass that can be ignited at a given implosion velocity U_{im}:

$$M_{\min} \text{ [mg]} = 2 \times 10^5 \frac{\alpha^3}{U_{im}^{12}} \tag{37}$$

Equation (31) yields the required minimum energy investment in the DT fuel,

$$E_{\min} \text{ [MJ]} = 10^3 \frac{\alpha^3}{U_{im}^{10}} \tag{38}$$

As might be expected, the exponents of α and U_{im} in the last formula coincide with those derived earlier by Murakami and Meyer-ter-Vehn [16] on the basis of the isobaric approximation. A major disagreement of this scaling with the Livermore results is in the value of the U_{im} exponent, which, according to Refs [3, 4], must be -5 instead of -10.

The thermonuclear energy gain with respect to the energy E invested in fuel can be evaluated as

$$G_f = \epsilon_{DT} f_b \frac{M}{E} \tag{39}$$

where $\epsilon_{DT} = 3.4 \times 10^5$ MJ/g is the specific fusion energy, and f_b is the burn fraction. If, following Refs [20, 21], we use a simple approximation:

$$f_b = \frac{H_c}{H_c + H_0}, \qquad H_0 = 7 \text{ g/cm}^2 \tag{40}$$

for the burn fraction, we calculate a family of gain curves shown in Fig. 3. Each of the three gain curves was obtained for a fixed value of U_{im}, marked as a curve label, by varying the fractional spark radius ξ_s; the remaining parameters of the model were fixed at

$$H_s T_s = 2 \text{ g}\cdot\text{cm}^{-2}\cdot\text{keV}, \qquad \alpha = 2, \qquad q = 1$$

The envelope of the three gain curves shown as the dashed line $G_f^* \propto E^{0.32}$ in Fig. 3 is the limiting gain curve. If f_b were constant, the limiting gain would scale as $G_f^* \propto E^{1/5}$. Since, however, H_c decreases with increasing U_{im} (see Eq. (34)), G_f^* falls off more steeply than $E^{1/5}$ with decreasing E.

Analytically, the limiting gain G_f^* in the case of ignition threshold (36) can be evaluated as follows:

From Fig. 3 we infer that the envelope of the gain curves for different values of U_{im} corresponds to $\xi_s \approx 0.2$, which implies $\Lambda_M \approx \Lambda_E \approx 300$ and $\Lambda_H \approx 6.0$. From Eq. (4) we find that, when

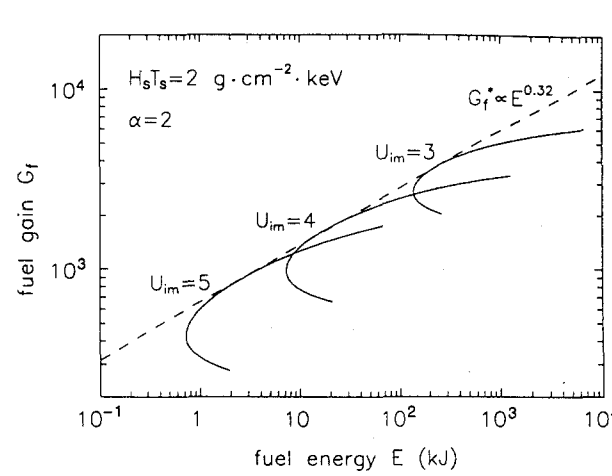

FIG. 3. Gain curves calculated from Eqs (30), (31), (39), and (40) for three values of the implosion velocity U_{im} = 3, 4 and 5 (in units of 10^7 cm/s) by varying the fractional spark radius ξ_s and assuming an ignition threshold of H_sT_s = 2 g·cm^{-2}·keV. Dashed line shows the limiting fuel gain G_f^*.

3×10^7 cm/s $\leq U_{im} \leq 5 \times 10^7$ cm/s, the values of H_c range from 2.5 g/cm^2 to 7 g/cm^2. Within this range, Eq. (40) can be approximated as

$$f_b = 0.16 H_c^{0.6} \tag{41}$$

where H_c is in g/cm^2. Then, from Eqs (30), (31), (34), and (41) we calculate

$$G_f^* = 1.5 \times 10^4 \left(\frac{E}{\alpha^3}\right)^{0.32} (H_s T_s)^{-0.36} q^{-2.64} \tag{42}$$

where E is in MJ, H_s in g/cm^2, T_s in keV. For $q = 1$, the only significant difference between Eq. (42) and the expression for G_f^* derived by Meyer-ter-Vehn [7] is the numerical factor, which is 1.6 times higher in our case, because of a more realistic pressure profile in the DT fuel at the time of stagnation.

3.2. Ignition criterion allowing for the inertia of the cold fuel

By its physical meaning, the ignition criterion based on fixed threshold values of T_s and H_s is adequate for a bare DT sphere but not for a thermonuclear spark surrounded by a layer of cold DT. As was explicitly noted in Refs [8, 14, 15], the ignition threshold for H_s is lowered by the tamping effect of the cold fuel and, in particular, decreases with the increasing density contrast ρ_c/ρ_s. Here, we reconsider the condition for spark ignition in terms of our model and demonstrate that an appropriate modification of this criterion has a considerable impact on the scaling of the minimum ignition energy E_{min} with the implosion velocity U_{im}.

In this section we restrict our discussion to the case of ignition at stagnation, i.e. we assume $q = 1$ when using the relationships from Section 2. From Eq. (8) we infer that the effective time of inertial confinement around the moment $t = 0$ is

$$\Delta t_c \simeq \frac{R_m}{U_\infty} = \frac{H_s}{\rho_s U_{im} \xi_s} \left(\frac{3}{8}\frac{\phi_E}{\phi_M}\right)^{1/2} \tag{43}$$

The DT fuel in the spark undergoes a thermonuclear flare whenever the net energy release during the period of confinement becomes comparable to the initial energy content of the DT plasma. Assuming flat temperature and density profiles across the spark region and taking into account the relevant heating and cooling mechanisms, we can approximately express this condition in the form of the following local relationship at the spark centre:

$$(Q_\alpha - Q_{br} - Q_{ec})\Delta t_c \simeq \frac{3}{2}(n_D + n_T + n_e)T_s \tag{44}$$

where

$$Q_\alpha = \epsilon_\alpha f_\alpha n_D n_T \langle\sigma v\rangle_{DT}$$
$$= 8.18 \times 10^{40} f_\alpha \rho_s^2 \langle\sigma v\rangle_{DT} \ [\text{erg}\cdot\text{cm}^{-3}\cdot\text{s}^{-1}] \tag{45}$$

is the alpha particle heating rate (ρ_s is in g/cm^3, $\langle\sigma v\rangle_{DT}$ in cm^3/s)

$$Q_{br} = 5.36 \times 10^{-24} n_e (n_D + n_T) T_s^{1/2}$$
$$= 3.11 \times 10^{23} \rho_s^2 T_s^{1/2} \ [\text{erg}\cdot\text{cm}^{-3}\cdot\text{s}^{-1}] \tag{46}$$

is the bremsstrahlung cooling rate, and

$$Q_{ec} = \zeta_{1/2}^2 \frac{\kappa_e T_s}{R_s^2} = 3.42 \times 10^{19} \frac{\rho_s^2 T_s^{7/2}}{H_s^2} \ [\text{erg}\cdot\text{cm}^{-3}\cdot\text{s}^{-1}] \tag{47}$$

is the cooling rate due to the electron heat conduction. In Eq. (45), f_α is the reduction factor due to the escape of alpha particles. By solving the transport equation in the approximation of straight trajectories, we calculate

$$f_\alpha = \begin{cases} 1 - [1 - (1-n)H_s/H_\alpha]^{\frac{1}{1-n}}, & H_s < (1-n)^{-1} H_\alpha \\ 1, & H_s \geq (1-n)^{-1} H_\alpha \end{cases} \tag{48}$$

at the centre of a uniform sphere; here, ϵ_α/H_α is the stopping power of the DT plasma for alphas at their birth energy $\epsilon_\alpha = 3.52$ MeV, and n is the exponent in the dependence of the stopping power, $d\epsilon_\alpha/dx \propto \epsilon_\alpha^n$. A good fit to more rigorous formulas [22] at 5 keV $\leq T_s \leq$ 30 keV, $\rho_s \simeq$ 30–50 g/cm^3 is obtained with $n = 0$ and

$$H_\alpha \ [\text{g/cm}^2] = 0.02 T_s^{1.2} \tag{49}$$

In contrast to the situation with Q_α and Q_{br}, we need more detailed assumptions on the temperature run across the spark region in order to evaluate the heat conduction losses Q_{ec}. In Eq. (47) we used the factor $\zeta_{1/2}^2 = 1.744$ calculated from the self-similar solution described in the Appendix; for the conduction coefficient κ_e, the Spitzer formula [23] with the Coulomb logarithm $\ln\Lambda = 5$ is used. For the subsequent discussion it will be convenient to rewrite Eq. (44) in the form

$$4.33 \times 10^{18} \frac{f_\alpha \langle\sigma v\rangle_{DT}}{T_s^2} \left(1 - \frac{Q_{br}}{Q_\alpha} - \frac{Q_{ec}}{Q_\alpha}\right) H_s T_s$$
$$= \frac{U_{im}\xi_s}{\beta_c} \left(\frac{\phi_M}{\phi_E}\right)^{1/2} \tag{50}$$

where we have introduced a numerical factor β_c of order unity, allowing for the uncertainty inherent in condition (44).

First of all, we notice that the left hand side of Eq. (50) is a function of T_s and H_s only (as long as the weak dependence of the Coulomb logarithms on ρ_s can be

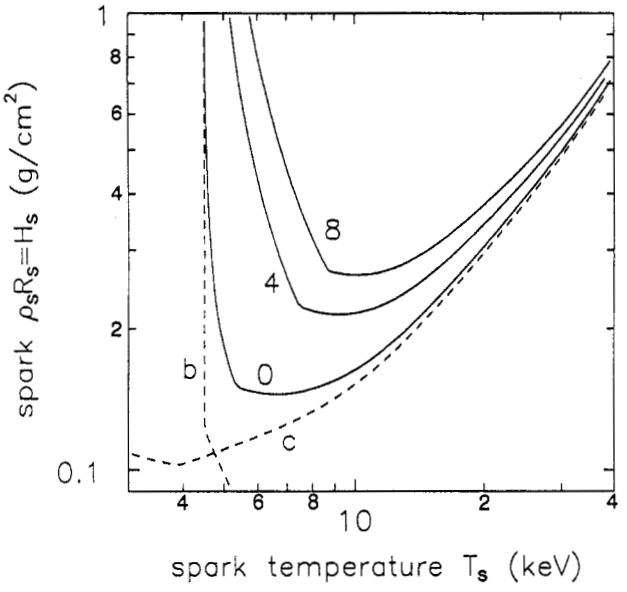

FIG. 4. Solid curves: ignition boundary for spark parameters as defined by Eq. (50) for three different values of the right hand side of this equation (in units of 10^7 cm/s). To the right of the dashed curve b, the alpha particle heating Q_α exceeds the bremsstrahlung cooling Q_{br}. Above the dashed curve c the alpha particle heating Q_α exceeds the heat conduction cooling Q_{ec}.

ignored), while its right hand side depends exclusively on U_{im} and ξ_s. Thus, for any pair of the U_{im} and ξ_s values, Eq. (50) defines an ignition boundary in the T_s, H_s plane (solid curves in Fig. 4). Generally, one can distinguish three branches along such an ignition boundary: (i) a radiative branch (approaching the dashed curve b in Fig. 4), where $Q_\alpha \approx Q_{br}$; (ii) a conduction branch (approaching the dashed curve c in Fig. 4), where $Q_\alpha \approx Q_{ec}$; and (iii) an inertial branch (above and between the dashed curves in Fig. 4), where $Q_{br} \ll Q_\alpha$ and $Q_{ec} \ll Q_\alpha$. In the limit of prolonged confinement, $U_{im}\xi_s \ll 10^7$ cm/s, the inertial branch disappears, the ignition boundary is defined by the heating and cooling equilibrium, $Q_\alpha = Q_{br} + Q_{ec}$, and the minimum threshold value of H_sT_s is independent of either U_{im} or ξ_s. In the opposite limit of high implosion velocities, $U_{im}\xi_s \gg 10^7$ cm/s, implying short confinement times, the product H_sT_s as a function of T_s has a minimum at the inertial branch, where the bremsstrahlung and conduction energy losses are negligible; asymptotically, the minimum value of H_sT_s becomes directly proportional to $U_{im}\xi_s(\phi_M/\phi_E)^{1/2}$.

Clearly, the above analysis based on condition (44) is only semi-quantitative. To find out precisely what ignition regime pertains to situations of interest here, a series of one dimensional hydrodynamic simulations starting at the time of stagnation has been carried out. The DEIRA code [18], employed for these simulations, has different electron and ion temperatures and accounts for the electron heat conduction with a proper flux limit. Separate diffusion equations for the energy densities of radiation and 3.5 MeV alpha particles are solved to approximate the energy transport by these agents. The initial state of the DT sphere in each numerical run was assigned according to the self-similar solution (1)–(9) at time $t = 0$. Numerical simulations have unequivocally demonstrated that, for spark temperatures 7 keV $\lesssim T_s \lesssim$ 12 keV, the ignition threshold for H_sT_s is directly proportional to the implosion velocity U_{im}, when $U_{im} \gtrsim 3 \times 10^7$ cm/s and $\xi_s \gtrsim 0.25$. Evaluating the proportionality factor from these simulations, we arrive at the ignition criterion:

$$\begin{cases} T_s \gtrsim 7 \text{ keV} \\ H_sT_s \text{ [g·cm}^{-2}\text{·keV]} \gtrsim 1.4U_{im}\xi_s\left(\dfrac{\phi_M}{\phi_E}\right)^{1/2} \end{cases} \tag{51}$$

It should be emphasized that Eq. (51) gives not just the ignition threshold for the product H_sT_s, but its minimum value along the ignition boundary, which typically occurs at $T_s \simeq$ 7–10 keV, and that this criterion applies only for high enough implosion velocities, $U_{im}\xi_s \gtrsim 10^7$ cm/s.

On substituting the ignition threshold for H_sT_s from Eq. (51) into Eqs (30) and (31), we obtain the following expressions for the minimum mass and energy of the DT fuel that can be ignited at a given implosion velocity:

$$M_{min} \text{ [mg]} = 446\,\frac{\alpha^3}{U_{im}^9}\,\Psi_M \tag{52}$$

$$E_{min} \text{ [MJ]} = 2.23\,\frac{\alpha^3}{U_{im}^7}\,\Psi_E \tag{53}$$

Here,

$$\Psi_M = \frac{[1 - (2\Omega)^{-1}\xi_s^2]^3}{(1 - \xi_s^2)^5}\left(\frac{\phi_E}{\phi_M}\right)^{9/2} \times \left(\phi_M + \frac{16}{15}\,\frac{\xi_s^3}{\Omega - \frac{1}{2}\xi_s^2}\right) \tag{54}$$

$$\Psi_E = \frac{[1 - (2\Omega)^{-1}\xi_s^2]^3}{(1 - \xi_s^2)^5}\left(\frac{\phi_E}{\phi_M}\right)^{7/2} \times \left(\phi_E + \frac{128}{75}\,\frac{\xi_s^5}{\Omega - \frac{1}{2}\xi_s^2}\right) \tag{55}$$

Similar to Λ_M and Λ_E, the functions $\Psi_M(\Omega, \xi_s)$ and $\Psi_E(\Omega, \xi_s)$ are practically equal and independent of Ω for $\Omega \gtrsim 1$. The plots of $\Psi_M(\xi_s) \approx \Psi_E(\xi_s)$ for $\Omega = 1$ and $\Omega = 2$ are shown in Fig. 2. Note that the scaling (53) is

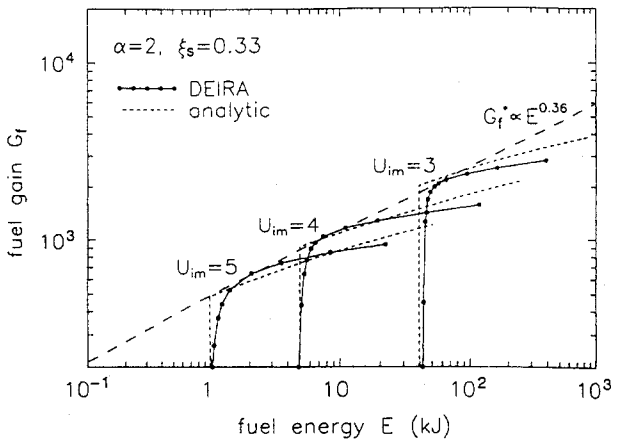

FIG. 5. Gain curves (solid curves with black dots) calculated for three implosion velocities with the one dimensional code DEIRA by varying H_s *for fixed* T_s *= 7 keV and* ξ_s *= 0.33. Short dash curves give the analytic results obtained from Eqs (39), (40), and (51). Long dash line is the limiting fuel gain* G_f^*.

much closer to the Livermore results [3, 4] than the Eq. (38) from the previous section.

Figure 5 shows the three gain curves calculated with the DEIRA code in the full treatment of the relevant physical processes for the values of the implosion velocity U_{im} = 3, 4, and 5 × 10^7 cm/s. Each gain curve was obtained by varying the spark areal density H_s; the fuel sphere was initialized according to the solution (1)–(9) at t = 0. The rest of the model parameters were fixed at

$$T_s = 7 \text{ keV}, \quad \alpha = 2, \quad q = 1, \quad \xi_s = 0.33$$

Analytic results, calculated by substituting the ignition criterion (51) into Eqs (30), (31), (34) and (39), are shown as the short dashed curves. Apparently, in what concerns the scaling of the minimum ignition energy E_{min} with U_{im}, a perfect agreement between the analytical model and the DEIRA simulations is observed. A slight deviation ($E_{min} \propto U_{im}^{-7.23}$) from the $E_{min} \propto U_{im}^{-7}$ law is due to a weak dependence of Ψ_E on Ω, which in its turn scales as U_{im}^{-2} (see Eq. (25)).

Equation (53) implies that, besides U_{im}, the minimum ignition energy E_{min} depends essentially on α and ξ_s. While the scaling $E_{min} \propto \alpha^3$ is perfectly reproduced by the hydrodynamic simulations, this is not quite the case for the dependence on ξ_s represented by function $\Psi_E(\xi_s)$. As explained above, the ignition criterion (51) fails at small $\xi_s \lesssim 0.2$, as the threshold value of H_sT_s approaches a finite limit for $\xi_s \to 0$. As a consequence, the ignition energy E_{min} considered as a function of ξ_s for fixed U_{im} and α has a minimum at $\xi_s \approx 1/3$. Also, one dimensional simulations indicate that beyond this minimum, at $\xi_s > 1/3$, $E_{min}(\xi_s)$ rises somewhat less steeply with ξ_s than is predicted by Eq. (55).

The limiting gain G_f^* can be calculated by using the same arguments as in Section 3.1. Now, the values of H_c given by Eq. (34) range from $\simeq 1.5$ g/cm^2 to $\simeq 2.5$ g/cm^2, and the burn fraction can be approximated as

$$f_b = 0.13 H_c^{0.8} \tag{56}$$

After the ignition threshold (51) has been substituted into Eq. (34), Eqs (39), (53), and (56) yield

$$G_f^* = 1.8 \times 10^4 \left(\frac{E}{\alpha^3}\right)^{0.4} \tag{57}$$

where E is in MJ. This scaling of G_f^* with E is not much different from $G_f^* \propto E^{0.32}$ calculated in Section 3.1 for fixed values of the product H_sT_s. As is shown in Fig. 5, the DEIRA simulations exhibit somewhat less steep dependence, $G_f^* \propto E^{0.36}$.

3.3. Limitations due to the hydrodynamic instabilities and drive asymmetries

The scaling laws (53) and (57) were derived solely on the basis of the ignition condition in inertially confined DT microspheres. They should apply in the most general case, when no other restrictions are imposed by, say, specific features of the drive scheme, hydrodynamic instabilities, fuel preheat, etc. In this section, we consider how these scaling relationships may be affected by the limitations due to the Rayleigh–Taylor instabilities and the large scale non-uniformities in the driving pressure.

To perform the necessary estimates, we have to make certain assumptions on the implosion scheme. Having in mind fusion capsules driven by thermal X rays, we assume that a DT shell of mass M_c in the initial solid state is surrounded by an ablator of mass

$$M_a = aM_c \tag{58}$$

Suppose also that the implosion occurs in the hydrodynamically most efficient way, i.e. all the ablator mass is evaporated by the end of implosion and the initial ablator/fuel mass ratio is near its optimal value $a \approx 4$–5 [24], for which the hydrodynamic efficiency is maximum.

We shall distinguish two phases of the implosion: the prepulse phase and the main pulse phase. In the prepulse phase illustrated in Fig. 6, the driving pressure rises from P_0 to its main pulse value, P_1, in such a way as to set the DT shell on the required isentrope with a given value of the parameter α. It is assumed that, by the end of this

phase (Fig. 6(c)), the inner edge of the fuel shell remains at practically its initial position, $r = R_1$. For simplicity, we also assume that the ablator obeys the same equation of state,

$$P = K\alpha\rho^{5/3} \tag{59}$$

as the DT fuel (which is approximately true for plastic ablators at high pressures, $P \gtrsim$ 50–100 Mbar), where K is a constant equal to 2.18 for P in Mbar and ρ in g/cm^3. At the onset of the main pulse (Fig. 6(c)), all the fluid elements of the fuel plus ablator shell have approximately the same acceleration, $g = \rho^{-1}(\partial P/\partial r)$, which by virtue of Eq. (59) implies

$$\rho(r) = \left(\frac{2}{5}\frac{g}{K\alpha}(r - R_1)\right)^{3/2} \tag{60}$$

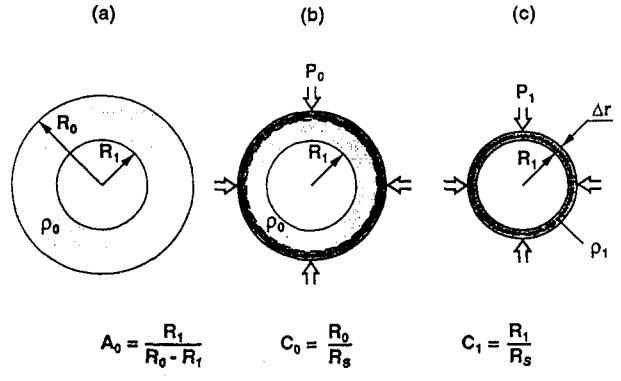

FIG. 6. Schematic view of the prepulse phase of implosion of a fusion capsule: (a) initial configuration of fuel plus ablator shell; (b) a relatively weak first shock controlling the entropy parameter α is launched into the shell; (c) the driving pressure reaches its peak value P_1 and the main pulse begins.

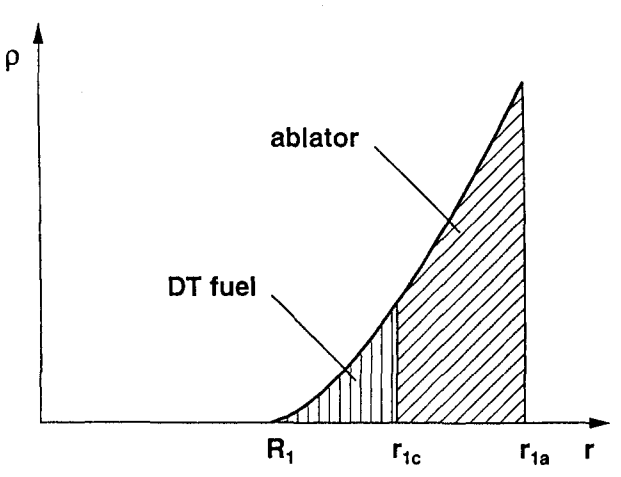

FIG. 7. Schematic view of radial density profile in the fuel plus ablator shell at the beginning of the main pressure pulse.

This density distribution is illustrated in Fig. 7. Since the thicknesses $r_{1c} - R_1$ and $r_{1a} - r_{1c}$ of the compressed DT and ablator shells are typically small compared to R_1, their masses can be expressed as

$$M_c = 4\pi R_1^2 \left(\frac{2}{5}\right)^{5/2} \left(\frac{g}{K\alpha}\right)^{3/2} (r_{1c} - R_1)^{5/2} \tag{61}$$

$$M_a + M_c = (1 + a)M_c = 4\pi R_1^2 \left(\frac{2}{5}\right)^{5/2} \left(\frac{g}{K\alpha}\right)^{3/2} (r_{1a} - R_1)^{5/2} \tag{62}$$

In general, the Rayleigh–Taylor instability at the ablation surface imposes limits on the inflight aspect ratios of ablatively imploded spherical shells [12, 13, 25]. In our case, the relevant inflight aspect ratios of the cold fuel and the ablator are, respectively,

$$A_c = \frac{R_1}{r_{1c} - R_1}, \quad A_a = \frac{R_1}{r_{1a} - r_{1c}} \tag{63}$$

Since we want to avoid the rupture of the ablator shell, a simple way of accounting for the constraints due to the Rayleigh–Taylor instability is to assume a certain fixed value of A_a. On the other hand, Eqs (58), (61), (62), and (63) yield

$$A_c = A_a[(1 + a)^{2/5} - 1] \tag{64}$$

which means that in optimized implosions with $a \approx$ 4–5 we have $A_c \approx A_a$; consequently, it can be assumed that the same limit applies to both A_a and A_c. Assuming that the DT shell attains the implosion velocity U_{im} after it has been accelerated during the main pulse phase with a constant acceleration

$$g = \frac{U_{im}^2}{R_1} \tag{65}$$

over a half of its initial radius R_1, from Eqs (59), (60), and (65) we evaluate the driving pressure:

$$P_1\ [\text{Mbar}] = 3.14 \times 10^3 \frac{1 + a}{A_c^{5/2}} \frac{U_{im}^5}{\alpha^{3/2}} \tag{66}$$

and the shell radius:

$$R_1\ [\text{mm}] = 0.136 A_c^{5/6} \frac{\alpha^{1/2} M_c^{1/3}}{U_{im}} \tag{67}$$

for the beginning of the main pulse phase; here, M_c is in mg.

Taken alone, an upper bound on the inflight aspect ratio A_c implies a lower limit on the driving pressure P_1 and an upper limit on the initial fuel radius R_1, but does not affect the scaling laws (53) and (57). The situation changes, however, when we take into account a limit on the radial convergence ratio. In our case, it is convenient to introduce two convergence ratios,

$$C_0 = \frac{R_0}{R_s} \quad \text{and} \quad C_1 = \frac{R_1}{R_s} \tag{68}$$

where R_0 and R_1 are, respectively, the outer ablator and the inner fuel radii of the fusion capsule in its initial state (see Fig. 6), and R_s is the spark radius at ignition. Non-uniformities in the driving pressure associated with low angular modes impose an upper limit of 30–40 on possible values of C_0 [13]; for simplicity, we assume that this limit does not depend on other implosion parameters.

From Eqs (67) and (68), we calculate

$$C_1 = 0.622 \frac{A_c^{5/6}}{q\xi_s} \left(\frac{(1 - \xi_s^2)\phi_M}{\phi_E^{3/5}} \right)^{5/6} \tag{69}$$

$$C_0 = C_1 \left[1 + \left(\frac{14.8}{A_c} \right)^{5/2} \frac{U_{im}^3}{\alpha^{3/2}} \right]^{1/3} \tag{70}$$

In deriving Eq. (70), it has been assumed that the initial density of the DT shell is 0.224 g/cm^3, while the initial ablator density is a factor of $a \approx 4$ higher, i.e. that the DT and the ablator shells have approximately equal initial volumes. The two convergence ratios C_0 and C_1 practically coincide when the initial thickness $R_0 - R_1$ of the fuel plus ablator shell is small compared to its radius R_1, or, in other words, when the initial aspect ratio,

$$A_0 = \frac{R_1}{R_0 - R_1} = \left\{ \left[1 + \left(\frac{14.8}{A_c} \right)^{5/2} \frac{U_{im}^3}{\alpha^{3/2}} \right]^{1/3} - 1 \right\}^{-1} \tag{71}$$

is large. The condition $A_0 \gg 1$ may be cast in the form

$$\alpha \gg \left(\frac{14.8}{A_c} \right)^{5/3} U_{im}^2 \tag{72}$$

Apparently, in the opposite limit of initially thick target shells, one should distinguish between C_0 and C_1. Note that, even when $A_0 \simeq 1$, the inflight aspect ratios, $A_c \approx A_a$, are typically much greater than unity.

A remarkable fact is that the ratio $C_1/A_c^{5/6}$ depends only on ξ_s and q. In the range of practical interest, $0.3 \lesssim \xi_s \lesssim 0.6$, the term in large parentheses in Eq. (69) is a weak function of ξ_s, and to a first approximation $C_1/A_c^{5/6}$ is inversely proportional to the product $q\xi_s$. For ignition at stagnation, when $q = 1$, fixed values of C_1 and A_c imply a fixed value of ξ_s. From this we conclude that the scalings (53) and (57) derived in Section 3.2 are not affected by the constraints due to the hydrodynamic instabilities and drive asymmetries when the initial aspect ratio of the fusion capsule $A_0 \gg 1$, i.e., when condition (72) is satisfied.

In the opposite case of initially thick capsule shells — a typical case for the values of α close to 1–2 — we should assume fixed values of A_c and C_0. As a consequence (see Eqs (70) and (69)), ξ_s becomes an increasing function of the ratio U_{im}^2/α. Since Ψ_E in Eq. (53) is an increasing function of ξ_s (Fig. 2), we obtain a weaker dependence of E_{min} on α and U_{im} than indicated by Eq. (53). Unfortunately, no well defined power law scaling of E_{min} and G_f^* with α and U_{im} can be established in this region, partly because the second term in brackets in Eq. (70) is of order unity and partly because the dependence of E_{min} on ξ_s in Eq. (53) is not a power law. This is clearly illustrated by Fig. 8, where three families of gain curves calculated with the DEIRA code for three different values of α are plotted. The one dimensional simulations have been conducted in the same way as described in Section 3.2. The only difference from the DEIRA curves in Fig. 5 is that each gain curve in Fig. 8 is characterized by its own value of the fractional spark radius ξ_s, calculated from Eqs (69) and (70), so as to keep $C_0 = A_c = 30$. These values of ξ_s are listed in Table I.

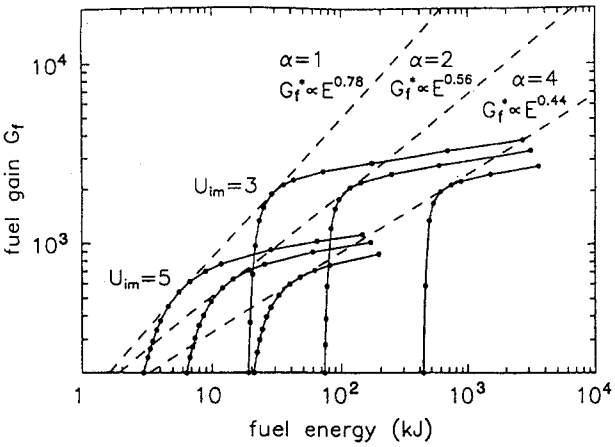

FIG. 8. Three families of gain curves calculated with the DEIRA code for three values of entropy parameter α. Each gain curve has its own value of the fractional spark radius ξ_s calculated from Eqs (69) and (70) for fixed values of the fuel inflight aspect ratio $A_c = 30$ and the capsule convergence ratio $C_0 = 30$. For different values of α we obtain different scalings of the limiting fuel gain G_f^* with the input energy E (dashed lines).

TABLE I. FRACTIONAL SPARK RADII ξ_s AS CALCULATED FROM Eqs (69) AND (70) FOR $C_0 = A_c = 30$, $q = 1$ AND DIFFERENT VALUES OF α AND U_{im}

U_{im} (10^7 cm/s)	$\alpha = 1$	$\alpha = 2$	$\alpha = 4$
3	0.531	0.457	0.408
4	0.602	0.517	0.447
5	0.657	0.571	0.490

From Fig. 8 we infer that the scaling of E_{min} with U_{im}, and of G_f^* with E changes from $E_{min} \propto U_{im}^{-3.6}$, $G_f^* \propto E^{0.78}$ for $\alpha = 1$ to $E_{min} \propto U_{im}^{-5.9}$, $G_f^* \propto E^{0.44}$ for $\alpha = 4$. Also, the scaling of E_{min} with α changes from $E_{min} \propto \alpha^{2.3}$ for $U_{im} = 3 \times 10^7$ cm/s to $E_{min} \propto \alpha^{1.4}$ for $U_{im} = 5 \times 10^7$ cm/s. To compare these results with the Livermore scaling, first of all note that in different Livermore publications the reader finds rather different formulas: $E_{min} \propto \alpha^3 U_{im}^{-6}$ in Ref. [2], $E_{min} \propto \alpha^4 U_{im}^{-5}$ in Ref. [3], $E_{min} \propto \alpha^{1.5} U_{im}^{-5}$ in Ref. [4]; the scaling of G_f^* ranges from $G_f^* \propto E^{2/3}$ in Refs [2, 3] to $G_f^* \propto E^{0.73}$ in Refs [1, 4]. In light of the above discussion, the most natural explanation for such a scatter would be that the Livermore results refer to initially thick shells, for which no well defined power law scaling can be established in general. A reasonable agreement between the predictions of the present model and the most recent scaling quoted by Lindl [4] is observed for values of α somewhere between 1 and 2, and $U_{im} \simeq 4 \times 10^7$ cm/s.

Finally, it is interesting to note that, after the value of ξ_s has been fixed by fixing C_0 and A_c, we are left with the product $H_s T_s$ as the only free parameter to construct a family of implosions corresponding to given values of α and U_{im} but with varying fuel mass M and igniting at stagnation (with $q = 1$; see Eqs [30, 31]). However, there is an upper limit to possible values of $H_s T_s$ that can be achieved in thermonuclear sparks by the time of stagnation because of the increasing role of radiation and heat conduction losses [19]. As a consequence, spark ignition of large enough DT masses can be arranged only in flight (before the stagnation), with parameter $q > 1$ — hence the need for this parameter in the general case.

4. CONCLUSIONS

In contrast with the analytic gain models for ICF targets published earlier, we have employed a self-similar solution of hydrodynamic equations to approximate the dynamical behaviour of the DT fuel near the time of ignition. This solution provides a suitable parametric description of spark ignited fuel configurations which is more accurate than the previous schemes based on either the isochoric [5, 6] or isobaric [7, 8, 11] approximations. We use this parametrization to examine the behaviour of the gain curves constructed for fixed values of the cold fuel entropy parameter α and implosion velocity U_{im}, and to derive the scaling of the ignition threshold E_{min} with α and U_{im}, and of the limiting fuel gain G_f^* with E (E is the energy invested in the DT fuel).

Our main result concerns the role of the ignition criterion in establishing the proper scaling of E_{min} and G_f^*. If, following the previous authors [5–7, 9–11], we assume fixed values of the spark temperature T_s and areal density $H_s \equiv \rho_s R_s$ at ignition, we recover the same scaling $E_{min} \propto \alpha^3 U_{im}^{-10}$ [16], $G_f^* \propto E^{0.3}$ [7] as was obtained in the isobaric model; only the numerical factors are somewhat different. However, a fixed value of H_s is not an adequate criterion of inertial confinement for a thermonuclear spark surrounded by cold fuel because it does not account for the tamping effect of the latter. We find instead that, along the relevant portion of the ignition boundary, the threshold value of the product $H_s T_s$ is directly proportional to the implosion velocity U_{im}. As a result, we derive the scaling $E_{min} \propto \alpha^3 U_{im}^{-7}$, which is confirmed by the one dimensional simulations with the DEIRA code and is in better agreement with the Livermore scaling [4] than the results of the isobaric model.

The effect of stability and symmetry constraints on the scaling of E_{min} and G_f^* is investigated by assuming fixed values of the ablator inflight aspect ratio A_a and the full convergence ratio C_0. It is shown that the scaling in question is not affected at all in the limit of large initial aspect ratios of fusion capsules $A_0 \gg 1$, but becomes ill defined when $A_0 \simeq 1$. In particular, the scaling of G_f^* with E in the latter case turns out to be rather sensitive to the value of the entropy parameter α, and only for $\alpha \approx 1$–2 a fair agreement with the latest Livermore scaling [4] is observed. If this agreement is not spurious, it may be concluded that the stability and symmetry constraints should have a considerable effect on the gain scaling for the family of targets simulated at Livermore. On the other hand, the absence of comprehensive agreement implies that either these constraints cannot be adequately described by simply assuming constant values of A_a and C_0, or there are other physical effects (such as the fuel preheat by the hard part of X ray spectrum or suprathermal electrons [2]) that significantly modify the scaling derived in Section 3.2.

Appendix

SELF-SIMILAR SOLUTION FOR AN ISOBARIC THERMONUCLEAR SPARK DISSIPATED BY HEAT CONDUCTION

Consider a spherical bubble of hot gas surrounded by an infinite shell of the same gas at a very low temperature. The initial parameters of the bubble are assumed such that the sonic timescale $t_s = R/c_s$ is much shorter than the timescale $t_{ec} = T/\dot{T}$ of temperature decay due to the heat conduction into the cold surrounding. Then, the thermal decay of such a hot spot proceeds at a constant pressure

P and is governed by the equations of mass and energy balance:

$$\frac{\partial \rho}{\partial t} + \frac{1}{r^2}\frac{\partial}{\partial r}(\rho u r^2) = 0 \tag{73}$$

$$\frac{\partial \epsilon}{\partial t} + u\frac{\partial \epsilon}{\partial r} + \frac{P}{\rho}\frac{1}{r^2}\frac{\partial}{\partial r}(ur^2) = \frac{1}{\rho r^2}\frac{\partial}{\partial r}\left(r^2\kappa\frac{\partial T}{\partial r}\right) \tag{74}$$

Assuming an ideal gas equation of state,

$$P = K\rho T, \qquad \epsilon = \frac{1}{\gamma - 1}\frac{P}{\rho} = \frac{KT}{\gamma - 1} \tag{75}$$

and making use of the condition P = const, we can integrate the energy equation (74) and reduce it to the condition of zero net flux of enthalpy:

$$\frac{\gamma}{\gamma - 1}Pu - \kappa\frac{\partial T}{\partial r} = 0 \tag{76}$$

By eliminating the velocity u between Eqs (73) and (76), we obtain an effective 'conduction' equation

$$\frac{\partial T}{\partial t} = \frac{\gamma - 1}{\gamma P}\frac{T^2}{r^2}\frac{\partial}{\partial r}\left(r^2\frac{\kappa}{T}\frac{\partial T}{\partial r}\right) \tag{77}$$

governing the temperature evolution in the hot bubble, which is quite distinct from the usual equation of heat conduction.

If heat conduction is the only mechanism of energy dissipation, the total energy in the bubble

$$E = \frac{1}{\gamma - 1}P\frac{4\pi}{3}R^3 \tag{78}$$

should be conserved; hence, for constant pressure P, the radius of the bubble R remains constant, as well. The hot bubble decays by ablating inwardly the surrounding cold matter: its mass increases and the temperature goes down. Accordingly, having assumed a power law dependence,

$$\kappa = \kappa_0 T^n \tag{79}$$

for the heat conduction coefficient, we look for a self-similar solution of Eq. (77) in the form

$$T(t, r) = T_0(t)\tau(\zeta), \qquad \zeta = \frac{r}{R_*} \tag{80}$$

TABLE II. THE VALUES OF ζ_0 AND $\zeta_{1/2}$ FOR DIFFERENT n IN THE SELF-SIMILAR SOLUTION (80)–(82)

n	0	1	2	2.5	3	6
ζ_0	3.2737	2.0149	1.5617	1.4247	1.3181	0.96475
$\zeta_{1/2}$	1.8467	1.5946	1.4006	1.3204	1.2495	0.95815

where R_* is a constant length scale. The eigenfunction $\tau(\zeta)$ is supposed to be normalized to $\tau(0) = 1$, so that $T_0(t)$ is the temperature at the bubble centre. The separation ansatz for Eq. (77) is

$$\frac{\dot{T}_0}{T_0^{n+2}}\frac{\gamma P R_*^2}{(\gamma - 1)\kappa_0} = \frac{\tau}{\zeta^2} = (\zeta^2\tau^{n-1}\tau')' = -1 \tag{81}$$

Here we used the freedom associated with the choice of R_* to set the separation constant equal to -1. The solution to the temporal part of Eq. (81) is

$$T_0(t) = T_{00}\left[1 + \frac{(\gamma - 1)(n + 1)\kappa_0 T_{00}^{n+1}}{\gamma P R_*^2}t\right]^{-\frac{1}{n+1}} \tag{82}$$

where $T_{00} = T_0(0)$. The eigenfunction $\tau(\zeta)$ is found numerically by solving the spatial part of Eq. (81) with the boundary conditions $\tau(0) = 1$, $\tau'(0) = 0$. It vanishes at $\zeta = \zeta_0$, which relates the bubble radius $R = \zeta_0 R_*$ to the length scale R_*. For practical applications, one might prefer to define the radius of a thermonuclear spark as the radius $R_{1/2} = \zeta_{1/2}R_*$ where the temperature drops to one half of its central value, i.e. where $\tau(\zeta_{1/2}) = 1/2$. The values of ζ_0 and $\zeta_{1/2}$ calculated for selected values of n are listed in Table II. For large n the difference between $\zeta_{1/2}$ and ζ_0 becomes negligible. The conduction cooling rate at the centre of the hot bubble can be expressed in terms of either R or $R_{1/2}$,

$$Q_{ec}(t) = -\frac{1}{r^2}\frac{\partial}{\partial r}\left(r^2\kappa\frac{\partial T}{\partial r}\right)\bigg|_{r=0} = \zeta_0^2\frac{\kappa_0 T_0^{n+1}}{R^2}$$

$$= \zeta_{1/2}^2\frac{\kappa_0 T_0^{n+1}}{R_{1/2}^2} \tag{83}$$

The isobaric approximation is justified for subsonic motions with $|u| \ll c_s$. Using Eq. (76) to evaluate the fluid velocity u, we can write this condition as

$$\frac{\gamma - 1}{\gamma P}\kappa\left|\frac{\partial T}{\partial r}\right| \ll \left(\frac{\gamma P}{\rho}\right)^{1/2} \tag{84}$$

For a thermonuclear spark in the DT plasma with Spitzer conductivity ($n = 5/2$, $\ln\Lambda = 5$) [23], Eq. (84) yields

$$H_s\ [\mathrm{g/cm^2}] \gg 1.59 \times 10^{-4} T_s^2 \tag{85}$$

which is always satisfied in the vicinity of the ignition boundary.

ACKNOWLEDGEMENTS

The author greatly appreciates stimulating discussions with J. Meyer-ter-Vehn. This work was partially supported by the Russian Fund for Fundamental Research, Grant No. 93-02-16906, and by the European Community Grant INTAS-93-2571.

REFERENCES

[1] STORM, E., et al., in Plasma Physics and Controlled Nuclear Fusion Research 1990 (Proc. 13th Int. Conf. Washington, DC, 1990), Vol. 3, IAEA, Vienna (1991) 99.
[2] LINDL, J.D., in From Fusion to Light Surfing (Lectures on Plasma Physics honoring John M. Dawson), Addison-Wesley, Redwood City, California (1991) 177.
[3] LINDL, J.D., et al., Phys. Today **45** (1992) 32.
[4] LINDL, J.D., paper presented at the Int. Symposium on Heavy Ion Inertial Fusion (Frascati, May 1993); Nuovo Cimento **106 A** (1993) 1467.
[5] KIDDER, R.E., Nucl. Fusion **16** (1976) 405.
[6] BODNER, S.E., J. Fusion Energy **1** (1981) 221.
[7] MEYER-TER-VEHN, J., Nucl. Fusion **22** (1982) 561.
[8] ATZENI, S., CARUSO, A., Nucl. Fusion **23** (1983) 1092.
[9] PIRIZ, A.R., WOUCHUK, J.G., Nucl. Fusion **32** (1992) 933.
[10] ATZENI, S., Part. Accel. **37&38** (1992) 495.
[11] MEYER-TER-VEHN, J., et al., paper presented at the Int. Symposium on Heavy Ion Inertial Fusion (Frascati, May 1993); Nuovo Cimento **106 A** (1993) 1883.
[12] VERDON, C.P., et al., Phys. Fluids **25** (1982) 1653.
[13] LINDL, J.D., in Inertial Confinement Fusion (Proc. Course and Workshop Varenna, 1988), Editrice Compositori, Bologna (1989) 595; 617.
[14] GUS'KOV, S.Yu., et al., Nucl. Fusion **16** (1976) 957.
[15] ATZENI, S., CARUSO, A., Nuovo Cimento **80** (1984) 71.
[16] MURAKAMI, M., MEYER-TER-VEHN, J., Nucl. Fusion **31** (1991) 1315.
[17] SEDOV, L.I., *Similarity and Dimensional Methods in* Mechanics, Nauka, Moscow (1981), Ch. VI, Section 15 (in Russian).
[18] BASKO, M.M., Nucl. Fusion **32** (1992) 1515.
[19] BASKO, M.M., Nucl. Fusion **30** (1990) 2443.
[20] BRUECKNER, K.A., JORNA, S., Rev. Mod. Phys. **46** (1974) 325.
[21] FRALEY, G.S., et al., Phys. Fluids **17** (1974) 474.
[22] BASKO, M.M., Fiz. Plazmy **10** (1984) 1195 (in Russian); Sov. J. Plasma Phys. **10** (1984) 689 (English translation).
[23] SPITZER, L., Jr., in Physics of Fully Ionized Gases, 2nd edn, Interscience, New York (1962) 144.
[24] MURAKAMI, M., NISHIHARA, K., Jpn. J. Appl. Phys. **26** (1987) 1132.
[25] TAKABE, H., et al., in Plasma Physics and Controlled Nuclear Fusion Research 1990 (Proc. 13th Int. Conf. Washington, 1990), Vol. 3, IAEA, Vienna (1991) 53.

(Manuscript received 23 March 1994
Final manuscript received 13 September 1994)